International Journal of Earth Sciences Knowledge and Applications
journal homepage: http://www.ijeska.com/index.php/ijeska
e-ISSN: 2687-5993

Research Article

https://doi.org/10.5281/zenodo.22165348

Geochemical Signatures and Mineralogical Composition of Basement Complex Lithologies in Afokpella, Southern Nigeria

Ezekiel Emetitiri[1], Anthony Ese Aladin[1]*, Ovie Odokuma-Alonge[1]

[1]*Department of Geology, University of Benin, Benin City, Edo State, Nigeria*

INFORMATION

Article history
Received 19 January 2026
Accepted 05 May 2026
Published 31 August 2026

Contact
*Anthony Ese Aladin
anthonyoriginal26@gmail.com (AEA)

How cite
Emetitiri, E., Aladin, A.E., Odokuma-Alonge, O., 2026. Geochemical Signatures and Mineralogical Composition of Basement Complex Lithologies in Afokpella, Southern Nigeria. *International Journal of Earth Sciences Knowledge and Applications* 8 (2), 243-262. https://doi.org/10.5281/zenodo.22165348.

Abstract
The Afokpella Area, located within the eastern extension of the Igarra Schist Belt in southwestern Nigeria, is underlain by a complex assemblage of Precambrian Basement complex rocks dominated by granites, charnockites, pegmatites, and marbles. This study investigates the geochemical and mineralogical characteristics of these rocks in order to constrain their petrogenesis, tectonic setting, and mineralization potential. Ten representative rock samples were collected and analyzed using X-ray fluorescence (XRF) for major oxide composition, complemented by petrographic thin-section analysis under a polarizing microscope. Results show that SiO_2 (55.82 wt.%), CaO (12.13 wt.%), Al_2O_3 (11.92 wt.%), and K_2O (5.21 wt.%) dominate the geochemical composition. Strong positive correlations were observed between Al_2O_3–SiO_2, Fe_2O_3–TiO_2, and LOI–CaO, while CaO shows strong negative correlation with SiO_2 and Al_2O_3, reflecting contrasting lithologic controls between silicate and carbonate rocks. Petrographic analysis reveals quartz, feldspars (microcline and plagioclase), biotite, hornblende, hypersthene, muscovite, and garnet as the dominant minerals. Geochemical discrimination diagrams classify the granitoids as high-K calc-alkaline to shoshonitic, peraluminous to slightly peralkaline, and emplaced within a passive continental margin setting. The marbles are characterized by very high CaO and LOI contents, indicating carbonate protoliths deposited in a shallow marine environment. Overall, the basement rocks of Afokpilla reflect crustal melting processes associated with Pan-African tectonism and possess significant industrial and economic mineral potential.

Keywords
Afokpella, Basement Complex Rock, Geochemistry, Petrography, Charnockite, Pan-African Orogeny

1. Introduction

The Nigerian Basement Complex forms part of the Pan-African mobile belt that lies east of the West African Craton and records a long history of crustal evolution spanning the Archean to Neoproterozoic eras.

Within this complex, the Igarra Schist Belt is notable for its diverse lithological assemblage, including metasedimentary rocks, marbles, quartzites, banded iron formations, and intrusive granitoids (Ajibade and Wright, 1989; Rahaman et al., 1988). Afokpella and its environs represent the eastern extension of the Igarra Schist Belt and host extensive granitoid intrusions, charnockitic rocks, pegmatites, and carbonate units that are economically important for cement production and construction materials.

Despite the industrial relevance of this area, detailed integrated geochemical and mineralogical studies remain

limited. This study aims to characterize the basement rocks around Afokpella using geochemical, petrographic, and statistical approaches in order to elucidate their origin, evolution, and mineralization potential.

2. Description of the Study Area

The study area is located in northeastern Edo State, Nigeria, between latitudes 7°18′N and 7°22′N and longitudes 6°22′E and 6°26′E, as shown in Fig. 1. It encompasses several communities, including Afokpella, Ojeaga, Okpoto, Kominio, and the BUA area. Access to the study area is primarily via Ogbida Road, which connects to Afowa Road, as well as through Winike Road leading to Afo–Okpella Road.

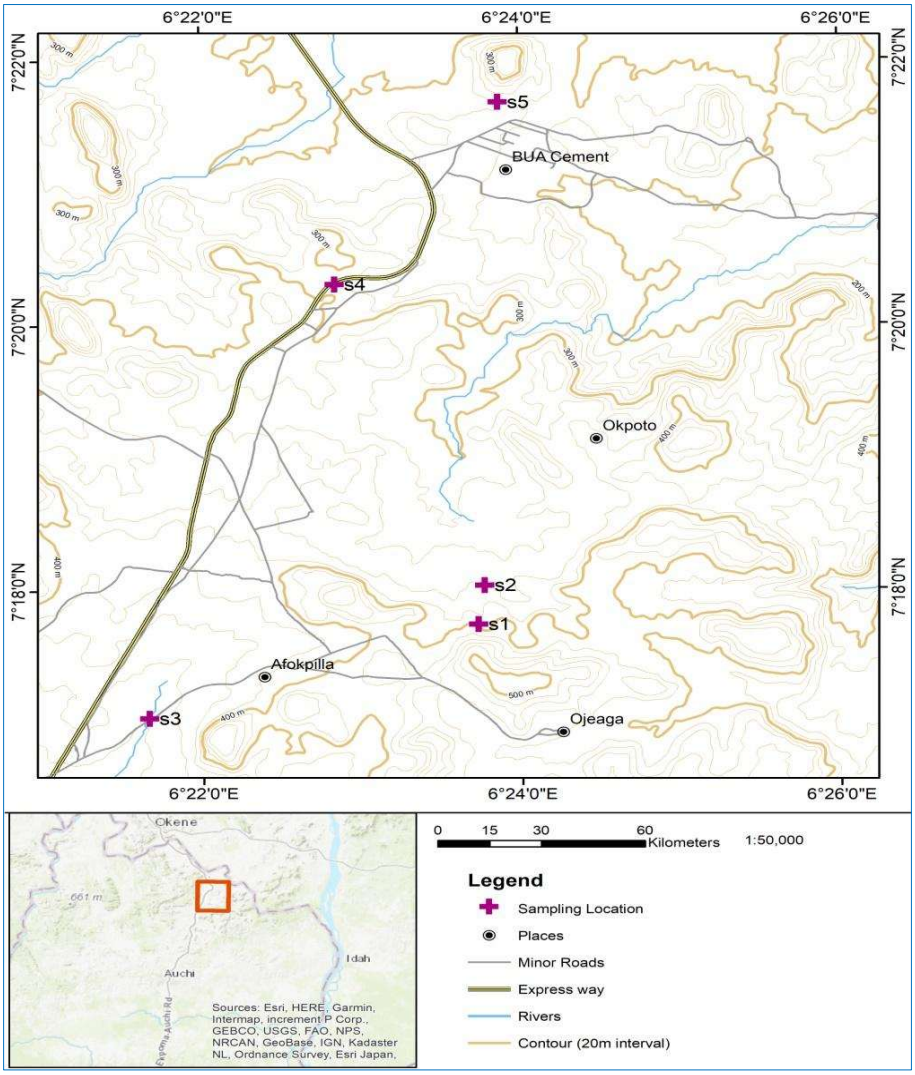

Fig. 1. Location map of the study area and sample locations

The predominant occupation of residents in Afokpella, Kominio, BUA, Okpoto, Ojeaga, Imiamune Afokpella, and surrounding communities is small-scale farming. Commonly cultivated crops include yam, maize, and cocoa. Agricultural activities are largely concentrated within valley areas, where loamy soils accumulate naturally, and provide favorable conditions for crop production. In addition, small-scale palm oil processing is practiced by local farmers. The area also supports quarrying activities, particularly the extraction of granite and quartzite for construction purposes. Afokpella is especially renowned for its abundant rock-based mineral resources, including limestone, calcium-rich deposits, granite, feldspar, talc, clay, and marble.

Climatically, the study area is situated within the tropical climatic zone, which is characterized by consistently high temperatures throughout the year. The region experiences two distinct seasons: the rainy season and the dry season. The rainy season typically spans from April to October, with a brief dry spell in August, while the mean annual rainfall ranges between 150 and 250 cm. Peak rainfall occurs between June.

3. Geological Setting

Geologically, the study area is underlain by a variety of crystalline Basement complex rocks, which includes biotite granite, biotite–hornblende granite, charnockite, migmatite–gneiss, calc-gneiss, marble, and pegmatite. These lithologic units are products of the Pan-African orogenic event, which involved widespread deformation, metamorphism, and

magmatic intrusions that affected the Nigerian Basement Complex around 600 Ma (Dada, 2006). The charnockitic rocks are typically coarse-grained and characterized by abundant orthopyroxene (hypersthene), reflecting high-grade metamorphic conditions or crystallization from deep-seated magmatic sources. The granitic bodies are predominantly felsic and silica-rich, representing intrusive magmatic phases emplaced during the Pan-African tectono-magmatic episode. In contrast, the marbles represent recrystallized carbonate rocks, derived from limestone protoliths originally deposited in shallow marine environments before undergoing regional metamorphism (Fig. 2).

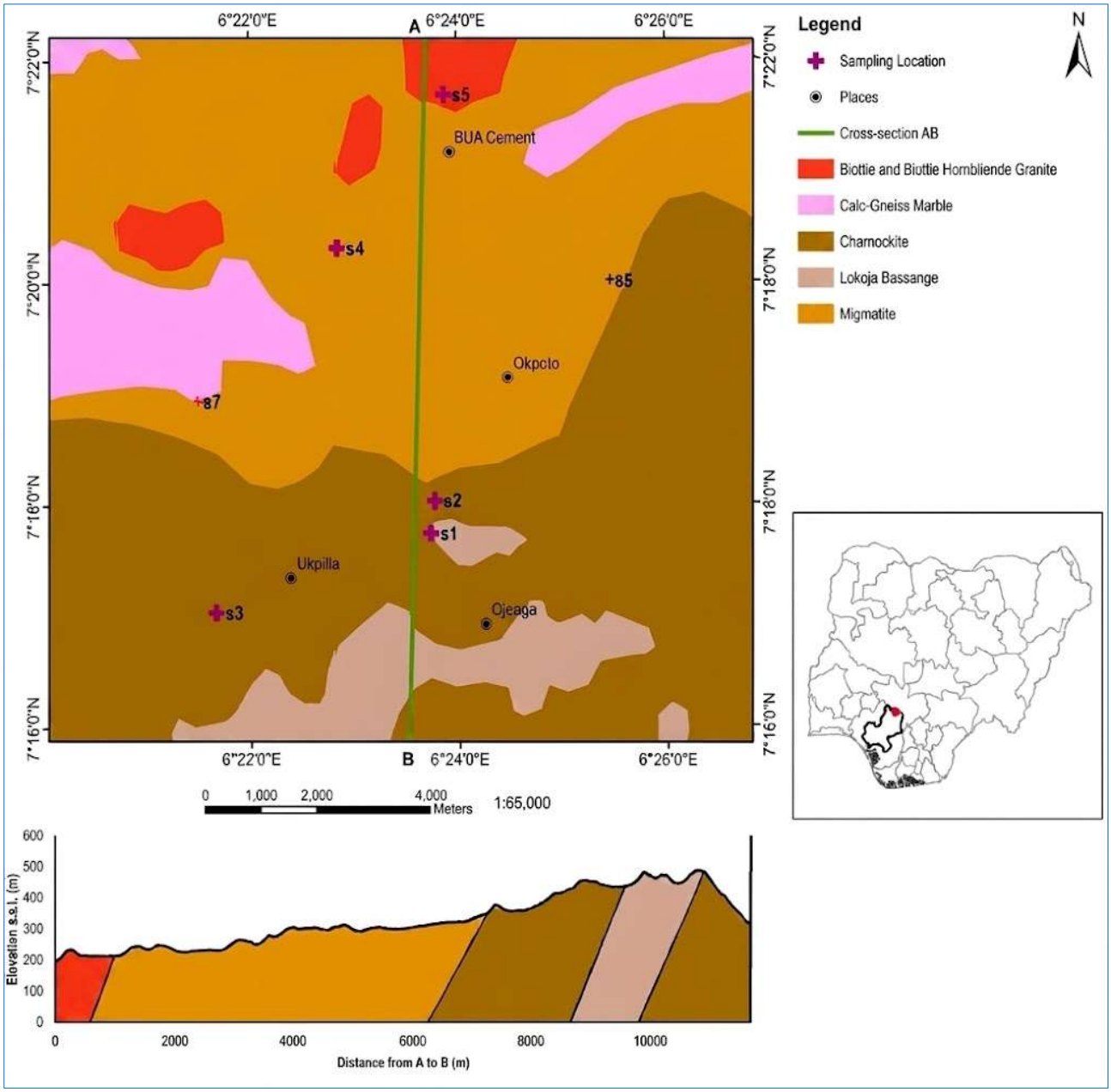

Fig. 2. Geological map of the study area

4. Materials and Methods

4.1. Field Mapping and Sampling

A total of ten (10) samples were collected out of which one was from a Biotite-granite host rock (Fig. 3). Sampling interval for the rock samples varied depending on the aerial extent of each outcrop and field environmental conditions encountered. Samples 1 and 2 were obtained from location 1; samples 3 and 4 from location 2; sample 5 from location 3; samples 6 and 7 from location 4; sample 8 from location 5; sample 9 from location 6; and sample 10 from location 7. The rock samples collected are Charnockite, Granite, Pegmatite, and Marble. The rock samples were crushed and pulverized into fine powder at the Department of Geology, University of Benin. Geological field mapping was conducted at a scale of 1:50,000 using GPS, compass clinometer, and standard geological tools. Ten representative rock samples comprising charnockite, granite, pegmatite, and marble were collected from different outcrops across the study area.

4.2. Geochemical Analysis

Whole-rock major oxide compositions were determined using X-ray fluorescence (XRF) spectrometry at Rolab Research and Diagnostic Laboratory, Ibadan. Samples were crushed, pulverized, sieved to <60 µm, and pressed into pellets prior to analysis.

4.3. Petrographic Analysis

Petrographic analysis was carried out using thin sections examined under plane-polarized light (PPL) and crossed-polarized light (XPL) with a petrographic microscope to determine the mineral composition, texture, and optical characteristics of the rock samples. The thin section was carried in University of Benin, Department of Geology, Benin City, Edo State.

Under plane-polarized light (PPL), the samples generally exhibited colourless to slightly brownish minerals with variable relief. Quartz grains appeared colourless, non-pleochroic, and displayed low relief, while feldspar minerals showed cloudy appearances due to alteration (sericitization). Some ferromagnesian minerals displayed pale brown to greenish hues, indicating the presence of biotite or amphibole. The grain boundaries ranged from sub-angular to sub-rounded, suggesting moderate transport and depositional reworking in some samples.

Fig. 3. Prepared rock samples label for analysis in the thin section laboratory

Table 1. Major oxides of silicate rock with statistical parameters

Major oxides	Charn 1	Charn 2	Biot. Grt 3	Biot. Grt 4	Biot. Grt 5	FnGrt 6	FnGrt 7	Pgm 8	Mean Conc. Wt.%	Std Dev.	Variances
SiO_2	61.56	62.74	70.7	72.9	71.5	72.74	71.7	72.72	69.570	4.651	438.274
TiO_2	1.81	1.65	0.02	0.01	0.01	0.02	0.42	0.02	0.495	0.776	0.476
Al_2O_3	13.97	12.9	17.19	15.15	15.47	15.15	13.65	15.17	14.831	1.318	19.612
Fe_2O_3	10.36	10.9	0.47	0.45	0.4	0.46	4.4	0.48	3.490	4.615	16.691
MnO	0.14	0.14	0.02	0.04	0.02	0.02	0.04	0.02	0.055	0.053	0.002
MgO	0.92	0.86	0.05	0.14	0.09	0.06	0.14	0.08	0.293	0.371	0.107
CaO	4.45	3.89	0.72	0.25	0.07	0.72	1.69	0.7	1.561	1.685	2.211
Na_2O	2.42	2.46	5.5	5.25	3.35	5.52	2.34	5.5	4.043	1.531	2.454
K_2O	3.99	4.2	8.22	5.5	8.05	8.2	5.65	8.2	6.501	1.869	4.863
P_2O_5	0.79	0.68	0.4	0.25	0.45	0.4	0.12	0.4	0.436	0.215	0.041

Under crossed-polarized light (XPL), quartz grains showed characteristic low-order grey to white interference colours and undulatory extinction in some cases, indicating strain effects. Feldspars displayed distinct twinning (especially albite twinning in plagioclase and cross-hatched twinning in microcline), confirming their identity. The interference colours of feldspar were generally low to moderate, while mica minerals exhibited bright interference colours and perfect cleavage. In some samples, extinction angles and birefringence variations were observed, which further helped in mineral identification.

Texturally, the rocks ranged from granular to moderately well-sorted, with interlocking grains in some samples indicating a crystalline origin, while others showed a more clastic texture typical of sedimentary environments. The presence of matrix materials in certain samples suggests partial compaction and cementation. Grain size varied from fine to medium, reflecting differences in depositional energy and source material.

Mineralogically, the samples are dominated by quartz and feldspar, with minor amounts of mica and accessory minerals. This mineral assemblage indicates a felsic composition, consistent with the geochemical results that showed high SiO_2 and Al_2O_3 contents. The relative abundance of feldspar suggests limited weathering or relatively short transport distances from the source rock.

4.4. Statistical Analysis

Descriptive statistics, correlation analysis, and hierarchical cluster analysis were applied to the geochemical dataset to evaluate elemental relationships and genetic associations.

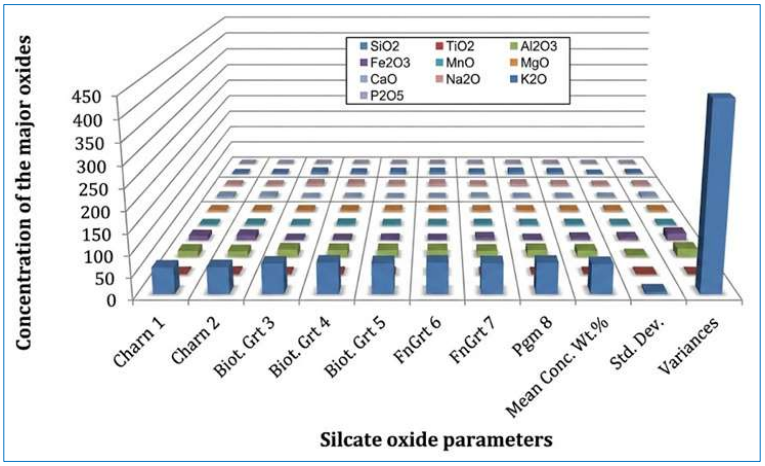

Fig. 4. Plot of concentration of major oxides against silicate rock oxide parameters (S 1-8)

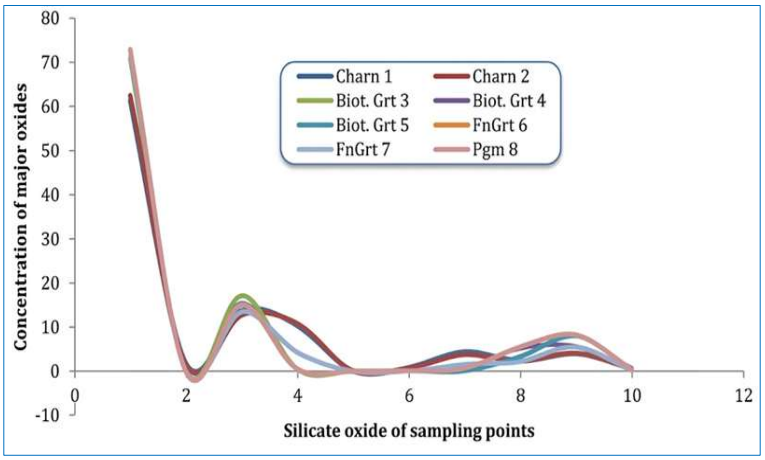

Fig. 5. Scatter diagram of concentration pattern of major oxides of silicate rock (S 1-8)

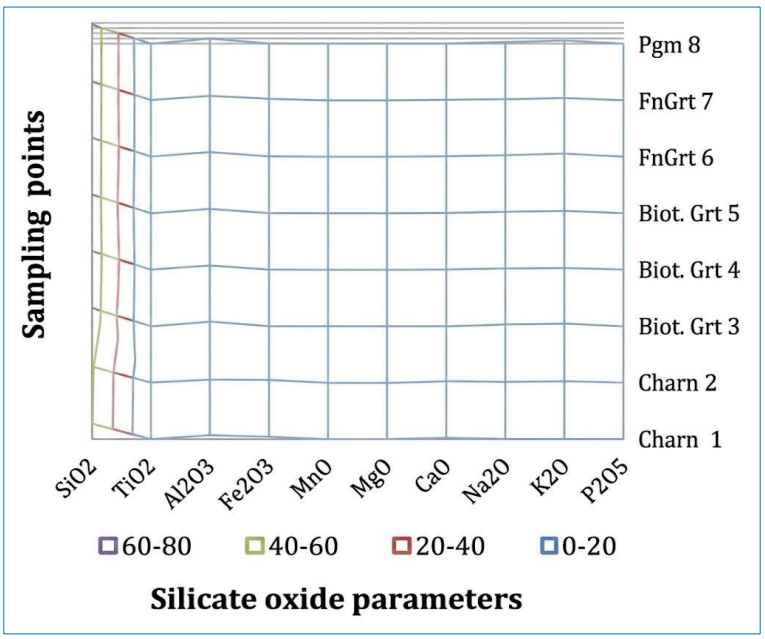

Fig. 6. Surface contour of major oxides of silicate rock (S 1-8)

5. Presentation of Results

5.1. Geochemical Characteristics

The oxides of silicate rock analysed for sample 1 to 8 include SiO_2, TiO_2, Al_2O_3, Fe_2O_3, MnO, MgO, CaO, Na_2O, K_2O and P_2O_5, The mean concentrations and corresponding standard deviations of these oxides are as follows: SiO_2 (69.570 ± 4.651 wt.%), TiO_2 (0.495 ± 0.776 wt.%), Al_2O_3 (14.831 ± 1.318 wt.%), Fe_2O_3 (3.490 ± 4.615 wt.%), MnO (0.055 ± 0.053 wt.%), MgO (0.293 ± 0.371 wt.%), CaO (1.561 ± 1.685 wt.%), Na_2O (4.043 ± 1.531 wt.%), K_2O (6.501 ± 1.869 wt.%) and P_2O_5 (0.436 ± 0.215 wt.%), as presented in Table 1. Figs. 4-6 show the oxide concentration of silicate rock.

The oxides of carbonate rock analyzed for sample 9 to 10 include SiO_2, TiO_2, Al_2O_3, Fe_2O_3, MnO, MgO, CaO, Na_2O, K_2O and P_2O_5, The mean concentrations and corresponding standard deviations of these oxides are as follows: SiO_2 (0.805 ± 0.134 wt.%), TiO_2 (0.015 ± 0.0.007 wt.%), Al_2O_3 (0.295 ± 0.318 wt.%), Fe_2O_3 (0.260 ± 0.113 wt.%), MnO (0.10 ± 0 wt.%), MgO (0.385 ± 0.049 wt.%), CaO (54.380 ± 0.523 wt.%), Na_2O (0.015 ± 0.007 wt.%), K_2O (0.045 ± 0.049 wt.%) and P_2O_5 (0.015 ± 0.07 wt.%), as presented in Table 2. Figs. 7-9 show the oxide concentration of carbonate rock.

For the silicate rocks (samples 1–8), the major oxides are dominated by SiO_2, with a mean value of 69.57 wt.%, followed by Al_2O_3 (14.83 wt.%), K_2O (6.50 wt.%), and Na_2O (4.04 wt.%). Other oxides such as Fe_2O_3, CaO, MgO, and TiO_2 occur in relatively lower concentrations. The relatively high standard deviations observed in some oxides, particularly Fe_2O_3 and CaO, suggest compositional variability within the silicate samples. Overall, the high silica and alumina contents indicate that the rocks are rich in quartz and feldspar minerals, reflecting a felsic to intermediate composition.

Table 2 Major. oxides of carbonate rock with statistical parameters

Major Elements %	Mar. NP 9	Mar. OP 10	Mean Conc. Wt.%	Std Dev.	Variances
SiO_2	0.71	0.9	0.805	0.134	0.018
TiO_2	0.01	0.02	0.015	0.007	0.000
Al_2O_3	0.52	0.07	0.295	0.318	0.101
Fe_2O_3	0.34	0.18	0.260	0.113	0.013
MnO	0.01	0.01	0.010	0.000	0.000
MgO	0.35	0.42	0.385	0.049	0.002
CaO	54.75	54.01	54.380	0.523	0.274
Na_2O	0.01	0.02	0.015	0.007	0.000
K_2O	0.01	0.08	0.045	0.049	0.002
P_2O_5	0.01	0.02	0.015	0.007	0.000

In contrast, the carbonate rock samples (samples 9–10) are characterized by extremely high CaO content (54.38 wt.%) and very low concentrations of SiO_2 (0.81 wt.%) and Al_2O_3 (0.30 wt.%). This composition confirms that these samples are predominantly carbonate in nature, likely composed mainly of calcite, with minimal silicate mineral contribution. The low variability in oxide concentrations suggests a more uniform composition compared to the silicate rocks.

Comparatively, the results clearly distinguish between the two rock types: silicate rocks are silica- and alumina-rich, while carbonate rocks are calcium-dominated. The elevated SiO_2 and Al_2O_3 values (>10 wt.%) in samples 1–8 indicate significant quartz and plagioclase feldspar content, whereas the low values in samples 9–10 reflect the absence of these minerals. Additionally, the relatively high K_2O content in the silicate samples points to the presence of potassic feldspar, confirming their feldspathic nature. From an applied perspective, the mineral composition of the silicate rocks suggests suitability for industrial uses such as glass and iron production, while the carbonate rocks, due to their high CaO content, may be suitable for cement and lime production.

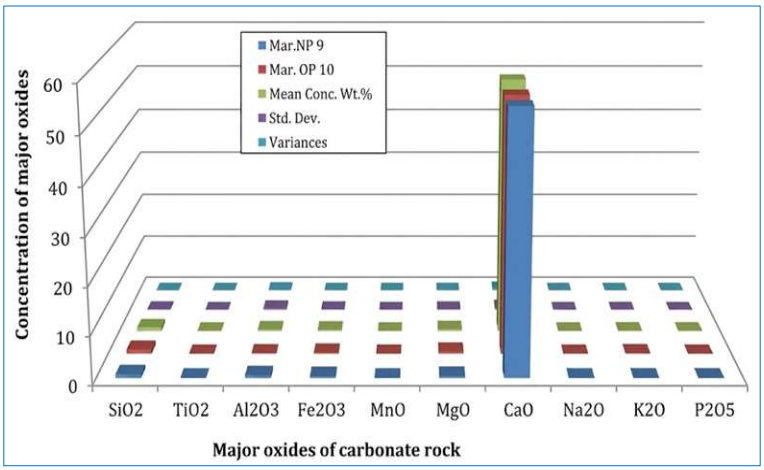

Fig. 7. Plot of concentration of Major oxides against oxides of carbonate rock (S 9-10)

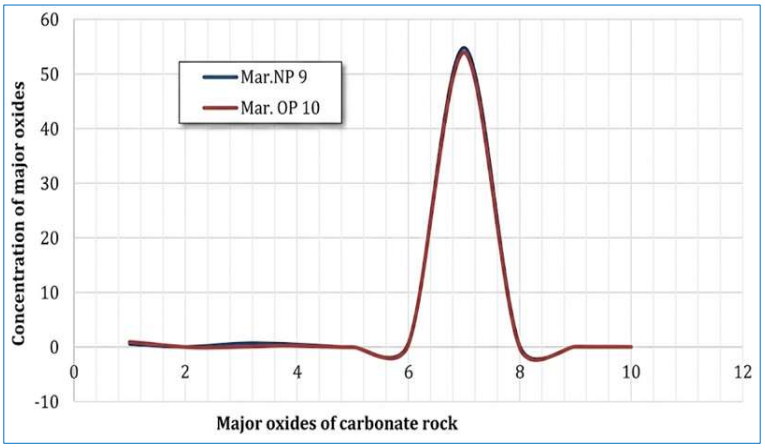

Fig. 8. Scatter diagram of concentration pattern of Major oxides of carbonate rock (S 9-10)

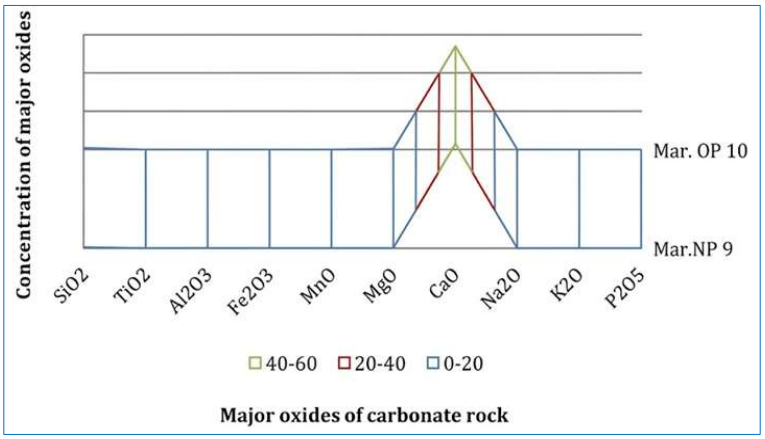

Fig. 9. Surface Contour of Oxides of carbonate rock (S 9-10)

5.2. Test of Significance of Observed Correlation Coefficients of Silicate Rock Major Oxides

The statistical relationships among the major oxides, as presented in Table 3, reveal significant geochemical associations within the dataset. A total of 55 pair wise correlations were analyzed. Out of these, ten exhibit very strong positive correlations at the 1% significance level ($P<0.01$), while eleven show strong positive correlations at the 5% level ($P<0.05$). Notable very strong positive relationships include $CaO–TiO_2$, $CaO–Fe_2O_3$, $Fe_2O_3–TiO_2$, $CaO–MnO$, $MnO–TiO_2$, $MnO–Fe_2O_3$, $MgO–TiO_2$, $MgO–Fe_2O_3$, and $MgO–MnO$, indicating close geochemical affinity among these oxides. Similarly, strong positive correlations at the 5% level are observed among $K_2O–Na_2O$, $K_2O–SiO_2$, $K_2O–Al_2O_3$, $Na_2O–SiO_2$, $Na_2O–Al_2O_3$, $Al_2O_3–SiO_2$, and several associations involving P_2O_5, suggesting shared mineralogical sources or similar geochemical behaviour.

Table 3. Correlation of Major Oxides of Silicate

	SiO_2	TiO_2	Al_2O_3	Fe_2O_3	MnO	MgO	CaO	Na_2O	K_2O	P_2O_5
SiO_2	1									
TiO_2	-0.9765	1								
Al_2O_3	0.5736	-0.7224	1							
Fe_2O_3	-0.9470	0.9892	-0.7835	1						
MnO	-0.9654	0.9871	-0.7182	0.9726	1					
MgO	-0.9786	0.9888	-0.6881	0.9642	0.9952	1				
CaO	-0.9540	0.9880	-0.7108	0.9825	0.9601	0.9604	1			
Na_2O	0.6779	-0.7419	0.7655	-0.7930	-0.6922	-0.6817	-0.7124	1		
K_2O	0.7618	-0.8462	0.7803	-0.8657	-0.8832	-0.8426	-0.8189	0.7177	1	
P_2O_5	-0.8626	0.7757	-0.2833	0.6914	0.7704	0.8233	0.7353	-0.3538	-0.4117	1

Conversely, five oxide pairs display very strong negative correlations at the 1% level, while sixteen show strong negative correlations at the 5% level. Prominent examples include $CaO–SiO_2$, $CaO–Al_2O_3$, $K_2O–CaO$, $LOI–SiO_2$, $Na_2O–MgO$, $K_2O–MgO$, and $P_2O_5–CaO$. These inverse relationships reflect compositional contrasts, particularly between carbonate-rich and silicate-dominated components. Additionally, several oxide pairs show weak positive and

negative correlations, alongside some perfect correlations, further highlighting the complexity of geochemical interactions. The strong positive associations–especially among Al_2O_3-SiO_2, Fe_2O_3-TiO_2, MnO-Fe_2O_3, K_2O-SiO_2, and K_2O-Al_2O_3–suggest co-genetic relationships, common source materials, or similar behaviour during weathering, transport, and deposition. In contrast, the pronounced negative correlation between CaO and SiO_2 clearly indicates lithological differentiation, pointing to the coexistence of carbonate-rich units and silicate-dominated rocks within the study area.

5.3. Principal Component Analysis

The Principal Component Analysis (PCA) results show that Component 1 is overwhelmingly dominant, with an eigenvalue of 7.945 explaining 99.32% of the total variance. This indicates that nearly all the variability in the dataset is controlled by a single underlying factor, suggesting strong similarity and correlation among the variables analyzed. The remaining components (Components 2–5) contribute negligible variance (<1%), meaning they do not significantly influence the dataset and can be disregarded in interpretation as shown in Table 4 and Fig. 10.

Table 4. Extraction method: Principal component analysis

Total Variance Explained							Communalities	
Component	Initial Eigenvalues			Extraction Sums of Squared Loadings				
	Total	% of Variance	Cumulative %	Total	% of Variance	Cumulative %		Extraction
1	7.945	99.318	99.318	7.945	99.318	99.318	Charn1	0.983
2	0.051	0.638	99.957				Charn2	0.982
3	0.002	0.019	99.976				BiotGrt3	0.995
4	0.001	0.015	99.991				BiotGrt4	0.997
5	0.001	0.008	99.999				BiotGrt5	0.997
							FnGrt6	0.996
							FnGrt7	0.999
							Pgm8	0.996

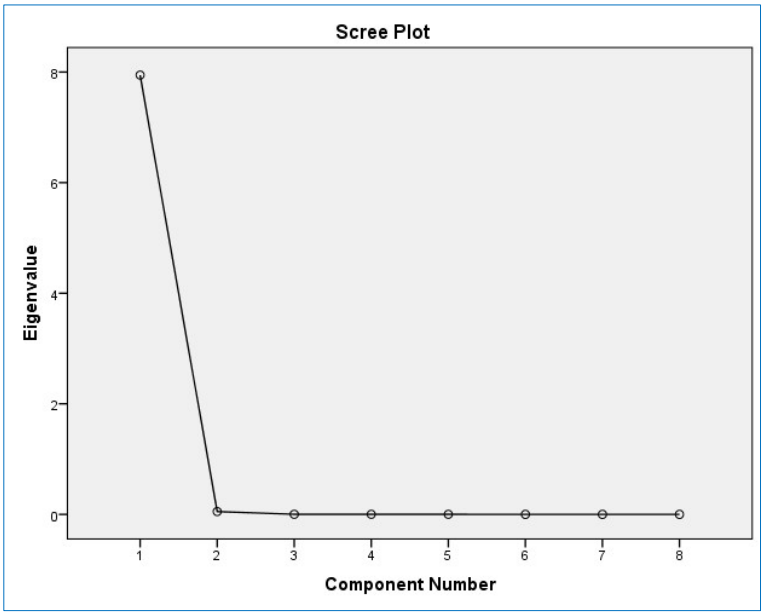

Fig. 10. Scree plot of eigenvalue against component number

The communalities values are very high (0.982–0.999) for all samples, indicating that the extracted component explains almost all the variability of each variable. This reflects a high degree of consistency and shared geochemical/petrological characteristics among the samples (Charnockite, Biotite Garnet, Fine Garnet, and Pegmatite). The results suggest that the rock samples are likely to share a common origin or similar geochemical evolution, with only minor differences between them as shown in Table 4 and Figure 9.

5.3. Hierarchy of Cluster (Major Oxides and Samples) Using Dendrogram of Average Linkage Between Elements and Sampling Points

The dendrogram clusters the samples and major oxides into two distinct groups, highlighting the degree of similarity and genetic relationships among them. One cluster groups CaO and LOI, as well as samples MarNP 9 and MarOP 10, indicating a very close geochemical affinity. This strong association suggests that CaO and LOI, and likewise MarNP 9 and MarOP 10, share a common source and were formed under similar depositional or post-depositional conditions.

The remaining oxides and samples form a separate cluster, implying differences in source materials, mineralogical composition, or geochemical evolution. These groupings, as illustrated in Figs. 11-12, reflect variations in lithology and geochemical processes that influenced the formation of the samples within the study area.

5.4. Geochemistry of Charnockite-Granite Association

From Table 5, the SiO_2 content of samples Ch1 and Ch2 ranges from 61.56 to 62.74 wt.%, which is lower than the values recorded for massive charnockite (MCh) and coarse charnockite (CCh), where SiO_2 ranges between 66.65 and 69.40 wt.%. This indicates moderate quartz content, suggesting that the charnockitic rocks are massive and moderately to coarse-grained in texture.

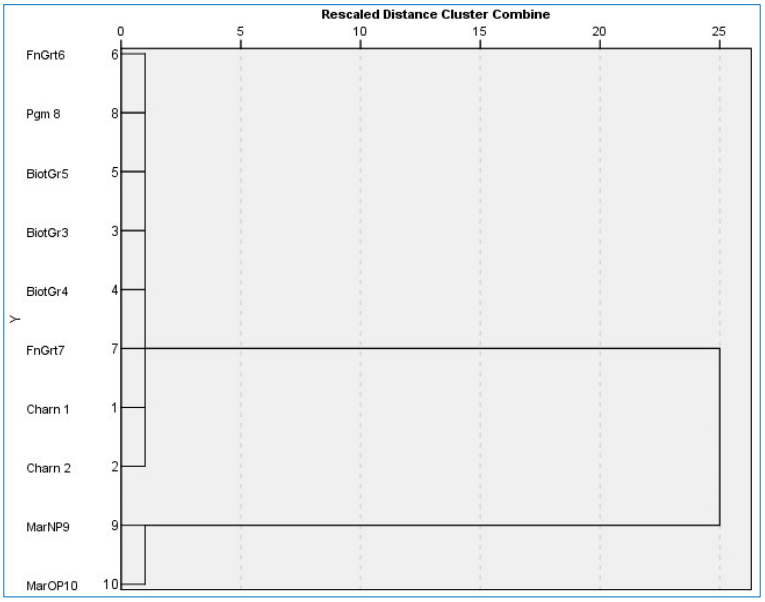

Fig. 11. Dendogram of average linkage between elements

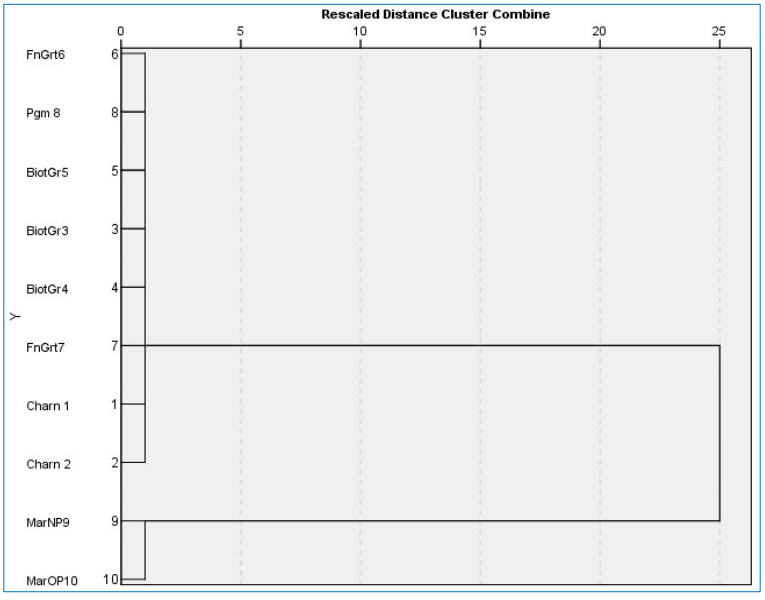

Fig. 12. Dendogram of average linkage between sampling points

The TiO_2 and Fe_2O_3 contents of Ch1 and Ch2 range from 1.61–1.81 wt.% and 10.36–10.90 wt.%, respectively, which are higher than the corresponding values for MCh and CCh (TiO_2: 0.62–0.70 wt.%; Fe_2O_3: 5.45–6.77 wt.%). Similarly, the CaO, Na_2O, and K_2O contents in Ch1 and Ch2 range from 3.89–4.45 wt.%, 2.42–2.46 wt.%, and 3.99–4.20 wt.%, respectively, exceeding those of MCh and CCh (CaO: 3.36–3.51 wt.%; Na_2O: 1.94–2.31 wt.%; K_2O: 2.33–2.35 wt.%). The MnO, MgO, and LOI contents of Ch1 and Ch2 range from 0.86–0.92 wt.%, 0.14 wt.%, and 0.01 wt.%, respectively. These values are generally lower than those recorded for MCh and CCh, which show MnO values of 1.32–2.12 wt.%, MgO of 0.13–0.18 wt.%, and LOI of 0.20–0.69 wt.%.

The P_2O_5 contents in the samples are higher than the comparative standard values, as illustrated in Table 5 and Fig. 13, which also depicts the overall concentration patterns of the major oxides.

From Table 6, only SiO_2 (71.91 wt.%), Al_2O_3 (15.32 wt.%), and K_2O (7.12 wt.%) have mean concentrations exceeding 5 wt.%, while the remaining oxides occur in lower proportions.

The SiO_2 content of biotite granite (samples 3–5) and fine-grained granite (samples 6–7) ranges from 70.70–72.90 wt.% and 71.70–72.74 wt.%, respectively. These values are higher than those reported for Granite G (65.35–66.00 wt.%; Adegbuyi, et al., 2017) and Granite H (Okeke, et al., 1988), confirming quartz as the dominant mineral phase.

Table 5. Comparison of oxides (Wt. %) in samples 1 and 2, with that of Charnockite–Granite Association (Ogunyele et al., 2020)

No	Major Elements wt. %	Charnockite 1	Charnockite 2	Medium Charnockite A (MCh) (Ogunyele, 2020)	Coarse Charnockite B (CCh) (Ogunyele, 2020)
1	SiO_2	61.56	62.74	66.65	69.40
2	TiO_2	1.81	1.65	0.70	0.62
3	Al_2O_3	13.97	12.90	14.36	13.72
4	Fe_2O_3	10.36	10.90	6.77	5.45
5	MnO	0.14	0.14	0.18	0.13
6	MgO	0.92	0.86	2.12	1.32
7	CaO	4.45	3.89	3.36	3.51
8	Na_2O	2.42	2.46	2.31	1.94
9	K_2O	3.99	4.20	2.35	2.33
10	P_2O_5	0.79	0.68	0.01	0.02
11	LOI	0.01	0.01	0.20	0.69
12	Na_2O+K_2O	6.41	6.66	4.66	4.27
13	K_2O/Na_2O	1.65	1.71	1.02	1.20
14	$CaO+ Na_2O+K_2O$	10.86	10.55	8.02	7.78
15	Al_2O_3/ Na_2O+K_2O	2.18	1.94	3.08	3.21
16	$Al_2O_3/CaO+ Na_2O+K_2O$	1.29	1.22	1.79	1.76

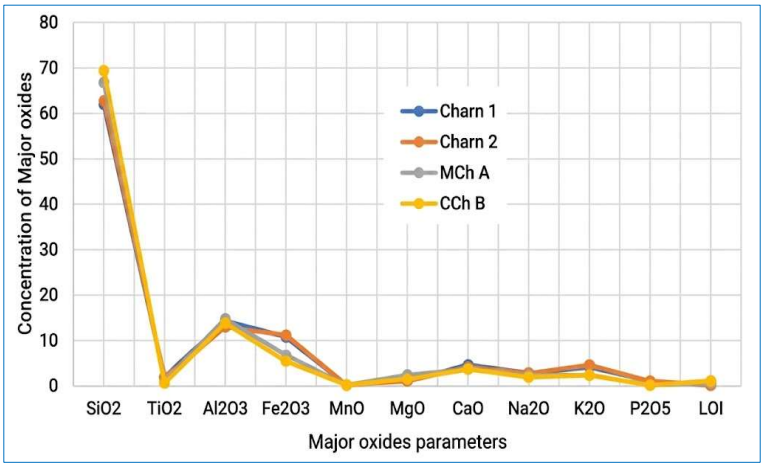

Fig. 13. Scatter diagram showing the concentration pattern of the major oxides of charnokite

Table 6. Comparison of Oxides (Wt.%) in sample 3, 4, 5, 6 and 7, with that of Idoani (Adegbuyi et al., 2017) and Igarra (Okeke et al., 1988)

Major Elements %	Biot. Grt 3	Biot. Grt 4	Biot. Grt 5	FnGrt 6	FnGrt 7	Mean concentration	Grt G Idoani (Adegbuyi, 2017)	Grt H Igarra (Okeke, 1988)
SiO_2	70.70	72.90	71.50	72.74	71.70	71.908	65.35	66.00
TiO_2	0.02	0.01	0.01	0.02	0.42	0.096	0.31	0.01
Al_2O_3	17.19	15.15	15.47	15.15	13.65	15.322	16.05	18.00
Fe_2O_3	0.47	0.45	0.40	0.46	4.40	1.236	1.72	0.82
MnO	0.02	0.04	0.02	0.02	0.04	0.028	0.07	0.06
MgO	0.05	0.14	0.09	0.06	0.14	0.096	2.19	2.00
CaO	0.72	0.25	0.07	0.72	1.69	0.69	1.89	1.92
Na_2O	5.50	5.25	3.35	5.52	2.34	4.392	3.56	3.66
K_2O	8.22	5.50	8.05	8.20	5.65	7.124	4.94	6.20
P_2O_5	0.40	0.25	0.45	0.40	0.12	0.324	0.11	0.01
LOI	0.20	0.69	0.75	0.20	0.31	0.43	0.00	0.00
Na_2O+K_2O	13.72	10.75	11.4	13.72	7.99	11.516	8.5	9.86
K_2O/Na_2O	1.49	1.05	2.40	1.48	2.41	1.62	1.39	1.69
$CaO+ Na_2O+K_2O$	14.44	11	11.47	14.44	9.68	12.206	10.39	11.78
Al_2O_3/ Na_2O+K_2O	1.25	1.41	1.36	1.10	1.71	1.33	1.89	1.82
$Al_2O_3/CaO+ Na_2O+K_2O$	1.19	1.38	1.35	1.05	1.41	1.25	1.54	1.53

The Al_2O_3 content ranges from 13.65–17.19 wt.%, falling within the standard values reported for Granites G and H. Elevated Al_2O_3 concentrations reflect the abundance of feldspar minerals, which are characteristic of felsic rocks. In contrast, MnO, MgO, Fe_2O_3, and CaO contents are relatively low, with ranges of 0.02–0.04 wt.%, 0.05–0.14 wt.%, 0.40–4.40 wt.%, and 0.07–0.14 wt.%, respectively. These values are below those of the reference granites

(Adegbuyi, et al., 2017; Okeke, et al., 1988), indicating a low proportion of ferromagnesian minerals.

The Na_2O and K_2O contents range from 2.34–5.52 wt.% and 5.50–8.22 wt.%, respectively, exceeding the standard values for Granites G and H. This enrichment suggests a significant presence of potassium feldspar and plagioclase, as shown in Table 6 and Fig. 14. Overall, the high SiO_2 content, combined with abundant feldspars and low ferromagnesian mineral content, indicates that the rocks are felsic in composition, dominated by quartz and feldspar, and deficient in minerals such as pyroxenes and amphiboles.

5.5. Petrogenesis of Charnockite–Granite Association

Igneous rocks in the study area were classified using the total alkali–silica (TAS) diagram based on $Na_2O + K_2O$ versus SiO_2 (Cox et al., 1979). The TAS classification identifies the samples as granitic compositions, with Biotite granite (BiotGrt 3–5) and fine-grained granite (FnGrt 6–7) plotting within the acidic field due to their high silica contents. This compositional affinity reflects the dominance of quartz, feldspar, and biotite, as illustrated in Fig. 15.

The K_2O/Na_2O versus SiO_2 discrimination diagram of Roser and Korsch (1986) indicates that the samples–Charnockite (Charn 1–2), BiotGrt (3–5), and FnGrt (6–7)–were emplaced within a passive continental margin tectonic setting, as shown in Fig. 16. This suggests derivation from evolved continental crust rather than active subduction-related environments.

Geochemical classification using the $Al_2O_3/(CaO + Na_2O + K_2O)$ (A/CNK) versus $Al_2O_3/(Na_2O+K_2O)$ (A/NK) diagram (Shand, 1943) reveals that the rock samples range from peralkaline to peraluminous compositions (Fig. 17). Peraluminous rocks, particularly those with intermediate to high silica contents, are commonly interpreted to be derived from crustal sources (Taylor and McLennan, 1981; Frost et al., 2001). Such peraluminous granites are typically classified as S-type granites, generated through partial melting of metasedimentary source rocks (White and Chappell, 1977).

The Na_2O+K_2O-CaO versus SiO_2 diagram places the samples within the shoshonitic to high-K calc-alkaline fields, as shown in Fig. 18. Shoshonitic and high-K calc-alkaline magmatic suites have been widely reported to be associated with gold–copper mineralization in several tectonic environments (Joplin, 1968).

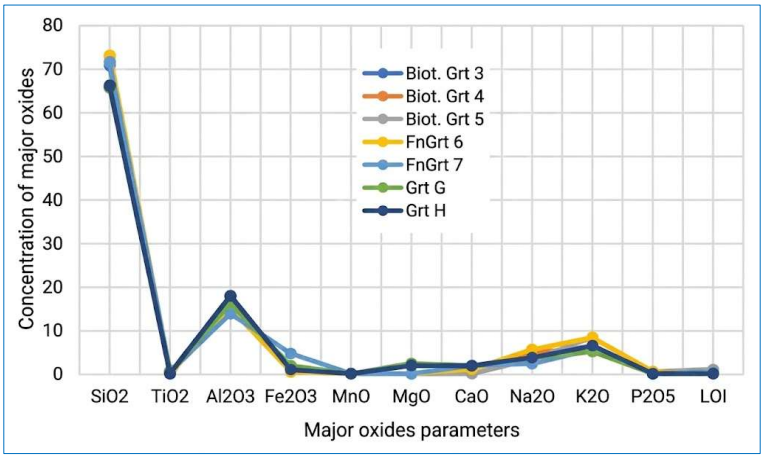

Fig. 14. Scatter diagram showing the concentration pattern of the major oxides of granite

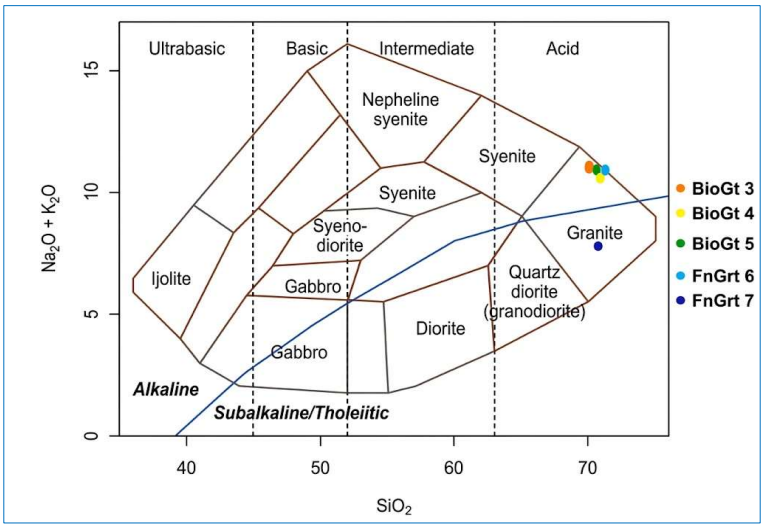

Fig. 15. TAS diagram of granite samples (after Cox et al., 1979)

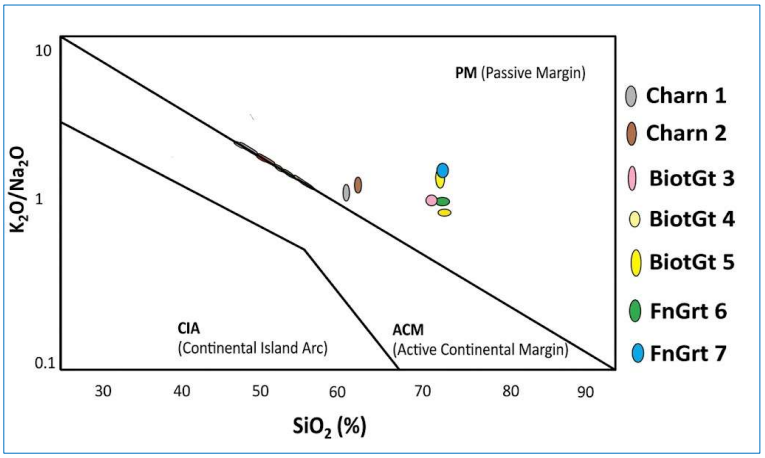

Fig. 16. K2O/Na2O versus SiO2 for samples in the study area. Source: Modified (after Roser and Korsch, 1986)

Furthermore, the Na_2O+K_2O-CaO versus SiO_2 classification scheme of Frost et al., (2001) indicates that the samples plot within the calc-alkalic to calcic (C-A to calcic) fields (Fig. 19). This geochemical signature is consistent with evolved felsic magmatism, reflecting significant fractional crystallization and crustal assimilation processes during magma evolution.

5.6. Photomicrograph of Granite Under Crossed Polarised Light (XPL)

Petrographic examination of thin sections under the polarizing microscope reveals that the dominant mineral constituents of the studied samples are quartz, feldspar minerals (including microcline), hornblende, and mica minerals such as muscovite and biotite.

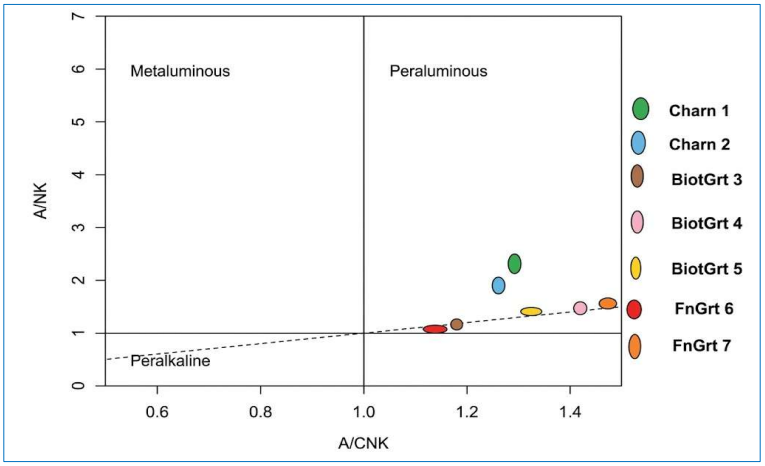

Fig. 17. $Al_2O_3/CaO+Na_2O+K_2O$ (A/CNK) vs Al_2O_3/Na_2O+K_2O (A/NK) diagram for Charnokite-Granite of study area (after Shand et al., 1943)

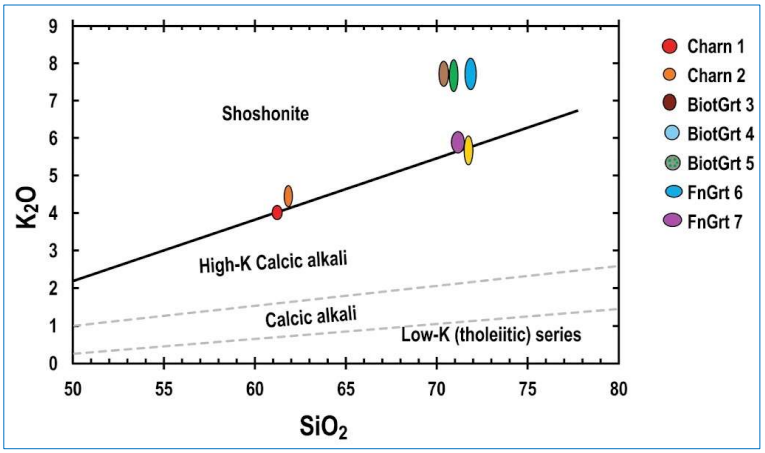

Fig. 18. K2O versus SiO2 diagram, the fields include the low-, medium- and high-K suite boundaries from Le Maitre et al., (1989) and the high-K–shoshonitic suite boundary from Peccerillo and Taylor (1976)

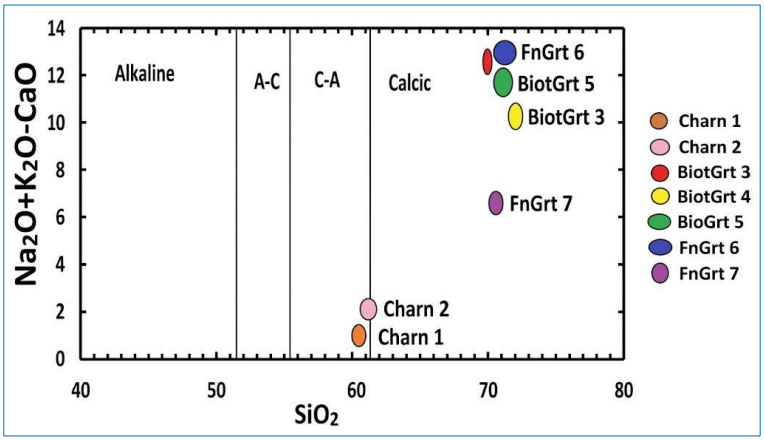

Fig. 19. Binary plot of Na_2O+K_2O-CaO versus SiO_2 for samples in the study area (Frost, et al., 2001)

Mineral identification was based on key optical properties observed under plane-polarized light (PPL) and crossed-polarized light (XPL), including relief, transparency, pleochroism, cleavage, and twinning.

Relief refers to the degree of contrast between a mineral and its surrounding medium, which is controlled by differences in refractive indices (McNamee and Gunter, 2014). Minerals such as quartz, albite, and microcline exhibit low relief, appearing weakly contrasted against the mounting medium. Quartz is an anisotropic mineral, displaying different refractive indices depending on the direction of polarized light. Microcline, potassium feldspar belonging to the monoclinic crystal system, also exhibits low relief. In pegmatitic samples, quartz behaves optically as a uniaxial mineral, characterized by two refractive indices and a single optical axis.

Transparent minerals allow light to pass through under plane-polarized light, whereas opaque minerals absorb light and appear dark under the microscope (Dyar and Gunter, 2008). Quartz and felsic minerals are transparent under PPL, while hornblende appears relatively darker and opaquer compared to quartz and feldspars due to its higher iron content. Pleochroism refers to the change in mineral color observed as the stage is rotated under plane-polarized light. Felsic minerals such as quartz and feldspars do not exhibit pleochroism (Dyar and Gunter, 2008). Under crossed polarizers, quartz displays characteristic interference colors as it is rotated. In charnockitic rocks, the presence of hypersthene is marked by distinct pleochroism, where the mineral exhibits varying shades depending on crystallographic orientation due to differential absorption of polarized light. Hypersthene also displays birefringence and interference colors under XPL. Quartz within charnockite appears colourless to slightly milky. In pegmatitic samples, garnet, being isotropic, remains uniformly dark under crossed polarizers, as shown in Figs. 20-21.

Cleavage describes a mineral's tendency to break along specific crystallographic planes of weakness (McNamee and Gunter, 2014). Microcline typically exhibits cleavage in two directions intersecting at approximately 90°, forming right angles. Under crossed polarizers, cleavage planes influence the display of interference colors as mineral orientation changes. Quartz lacks cleavage, and therefore its optical behavior remains consistent during stage rotation. In contrast, microcline shows variable interference colors due to the alignment of cleavage planes with the polarizer and analyzer. In charnockite, hypersthene commonly displays two well-developed cleavage directions at near-right angles. Biotite and muscovite, common in both charnockite and pegmatite, exhibit excellent basal cleavage, allowing them to split into thin sheets and display strong birefringence and vivid interference colors under XPL, as illustrated in Figs. 20-21 and Figs. 20-27.

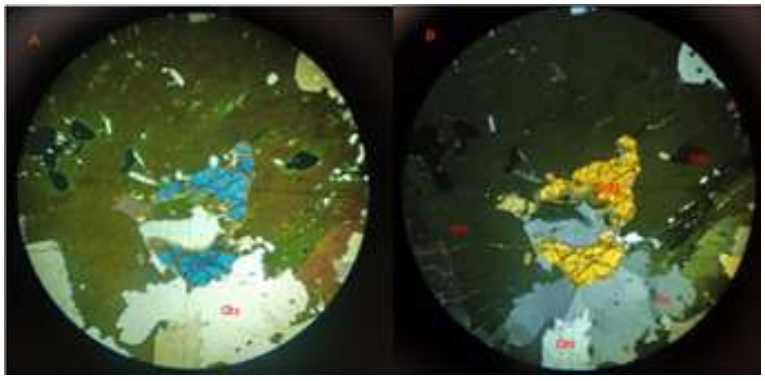

Fig. 20. Photomicrograph of Sample 1 Charnokite (a) under PPL and (b) under XPL x40; Op-Opaque, Qzt-Quartz, Mc-Microline, Biot-Biotite, Ort-Orthopyroxene(hypersthene), Mu-Muscovite

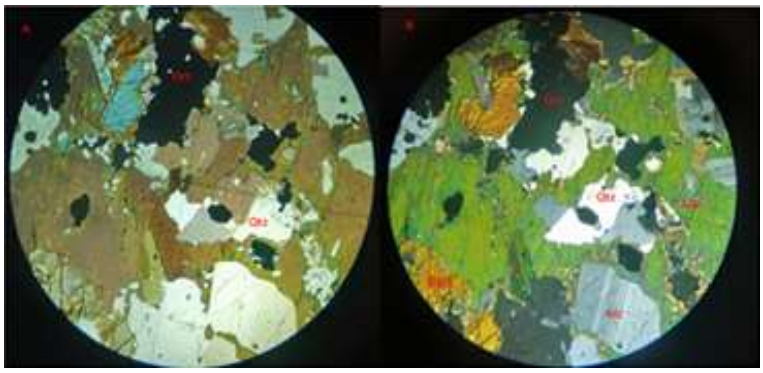

Fig. 21. Photomicrograph of Sample 2 Charnokite (a) under PPL and (b) under XPL x40; Op-Opaque, Qzt-Quartz, Mc-Microline, Ort-Orthopyroxene(hypersthene), Mu-Muscovite

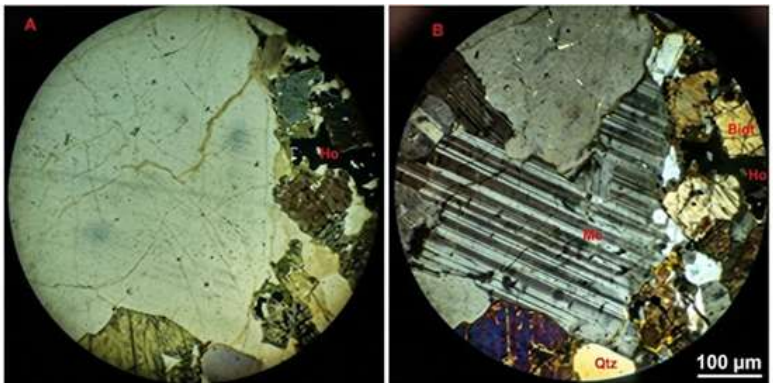

Fig. 22. Photomicrograph of Sample 3 Biotic Granite (a) under PPL and (b) under XPL x40; Op-Opaque, Qzt-Quartz, Mc-Microline, Biot-Boitite, Ho-Hornblende

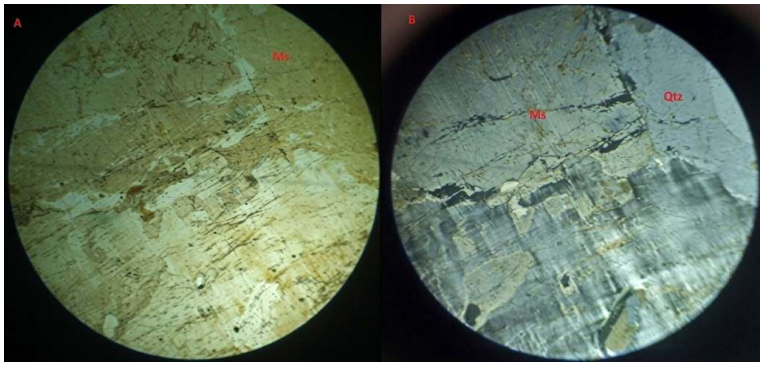

Fif. 23. Photomicrograph of Sample 4 Biotic Granite (a) under PPL and (b) under XPL x40; Op-Opaque, Qzt-quartz, Mc-Microline

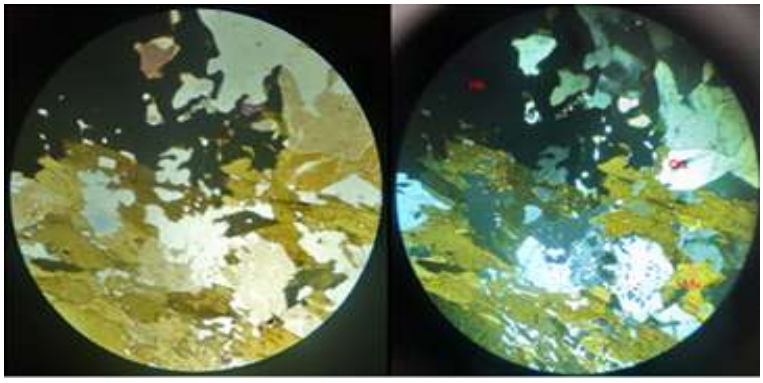

Fig. 24. Photomicrograph of Sample 5 Biotic Granite (a) under PPL and (b) under XPL x40; Op-Opaque, Qzt-quartz, Mc-Microline, Ho-Hornblede, Mu-Muscovite

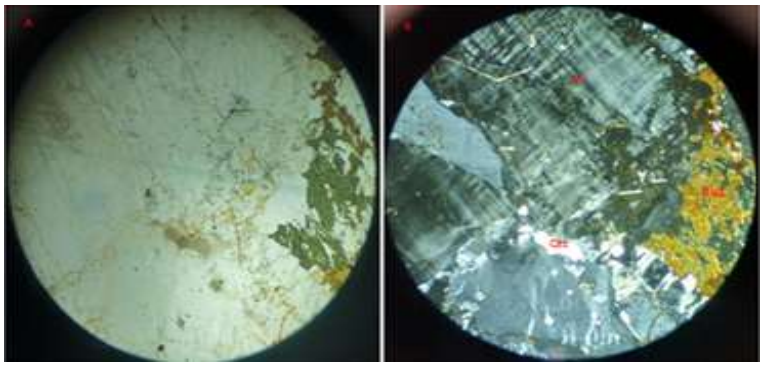

Fig. 25. Photomicrograph of Sample 6 fine-grained Granite (a) under PPL and (b) under XPL x40; Op-Opaque, Qzt-quartz, Mc-Microline, Biot-Biotite

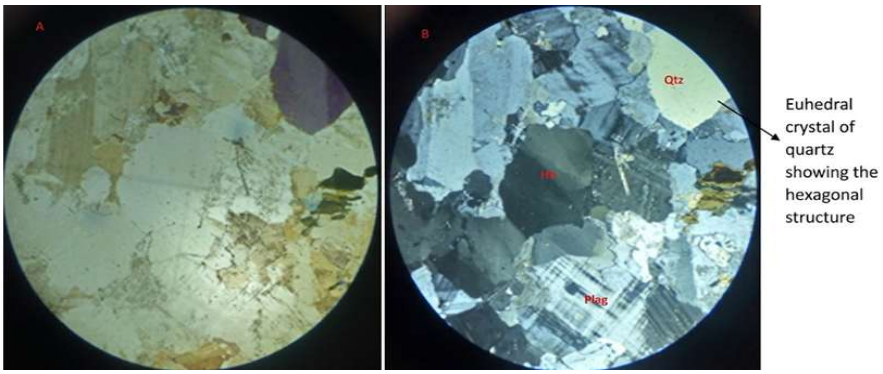

Fig. 26. Photomicrograph of Sample 7 fine-grained Granite (a) under PPL and (b) under XPL x40; Op-Opaque, Qzt-quartz, Mc-Microline, Ho-Hornblende

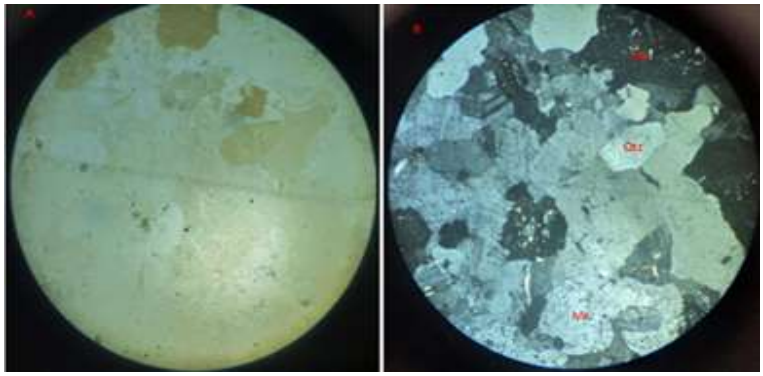

Fig. 27. Photomicrograph of Sample 8 Pegmatite (a) under PPL and (b) under XPL x40; Op-Opaque, Qzt-Quartz, Mc-Microline, Ga-Garnet

Twinning is defined as the regular intergrowth of two or more crystal segments related by symmetry operations such as reflection or rotation. Microcline is characterized by diagnostic crosshatch (tartan) twinning, which is clearly visible under crossed polarizers. Quartz in pegmatitic samples may exhibit subtle twin boundaries, observed as fine linear features accompanied by characteristic interference patterns. Although less common than in feldspars, biotite and muscovite in charnockitic rocks may also show twinning features, as shown in Figs. 20-21.

5.7. Bivariate Plots of Silicate Rock Oxides (SiO_2 Against Other Major Oxides)

Bivariate plot (Figs. 18–26) of Silicate oxides shows strong linear relationship with their linear formula and Coefficient of Regression (R^2). The bivariate plot of Al_2O_3, Na_2O and K_2O (0.2972, 0.2092 and 0.3013) against SiO_2 shows positive R^2. This indicates that they have close relationship with one another during period of deposition, coherent geochemical behaviour, possible common sources or co-precipitation processes and formation of the samples in the study area. But TiO_2, Fe_2O_3, MnO, MgO, CaO, P_2O_3 (-0.081, -0.094, -0.134, -0.102, -0.118, -0.249) show negative trend which indicates mineralogical differentiation and the lack of a direct genetic relationship between these oxides within the study area.

The R^2 values provide insight into the degree of geochemical association between the oxides and reflect their behaviour during the deposition and formation of the samples in the study area.

5.8. Geochemistry of Pegmatite and Marbles

Pegmatite is a type of igneous rock which is formed by slow crystallization at high temperature and pressure at depths and

exhibiting large interlocking crystals usually greater in size than 2.5 cm (Winter et al., 2014). Pegmatites usually occur as segregations within granites and as sharply discordant dikes intruding igneous and metamorphic rocks (London and Kontak, 2012).

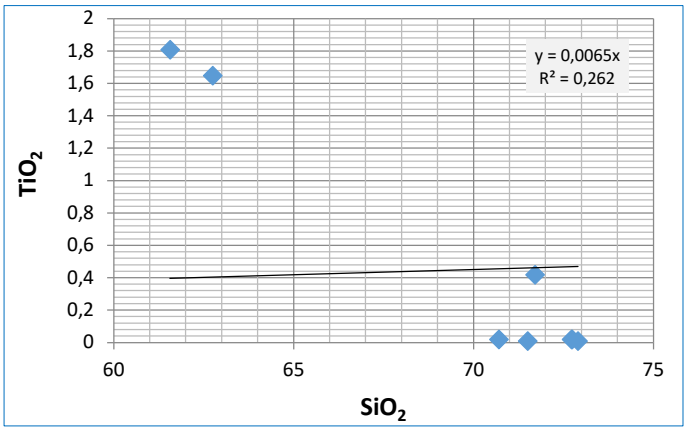

Fig. 28. SiO_2 against TiO_2

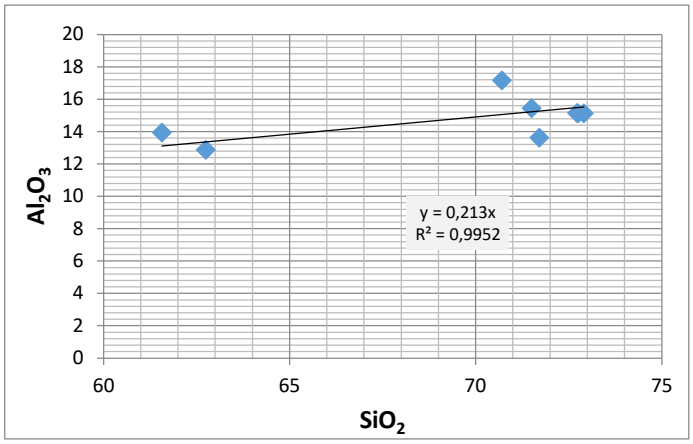

Fig. 29. SiO_2 against Al_2O_3

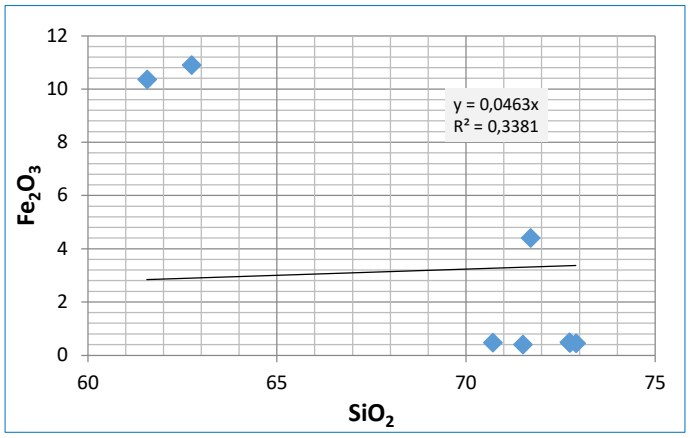

Fig. 30. SiO_2 against Fe_2O_3

The wt.% of SiO_2, Al_2O_3, Na_2O and K_2O are greater than 5 wt. % and the other are less than 5wt.%. The dominant major oxides are SiO_2, followed by Al_2O_3 and K_2O. This indicates the present of high quartz and alumina content. The value of alkaline content is low because of the low wt.% of K_2O, Na_2O and Ca_2O as shown in Table 7 and Fig. 37.

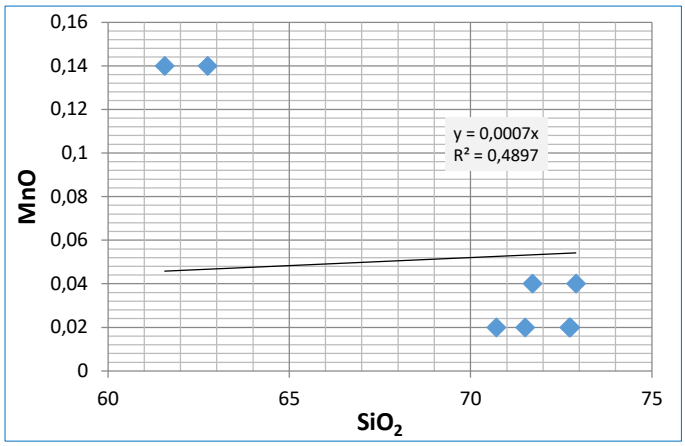

Fig. 31. SiO_2 against MnO

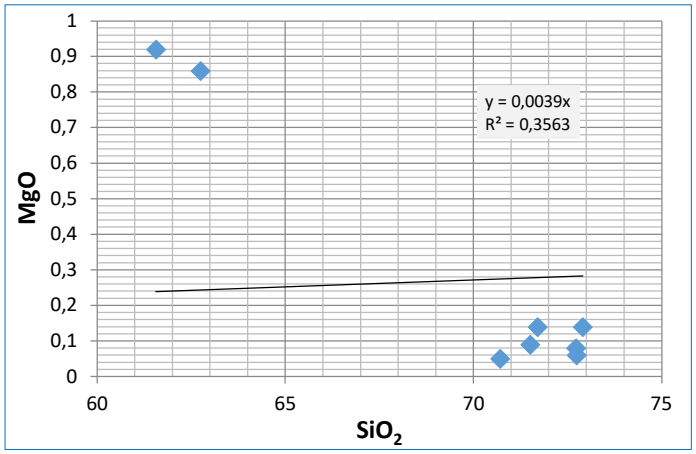

Fig. 32. SiO_2 against MgO

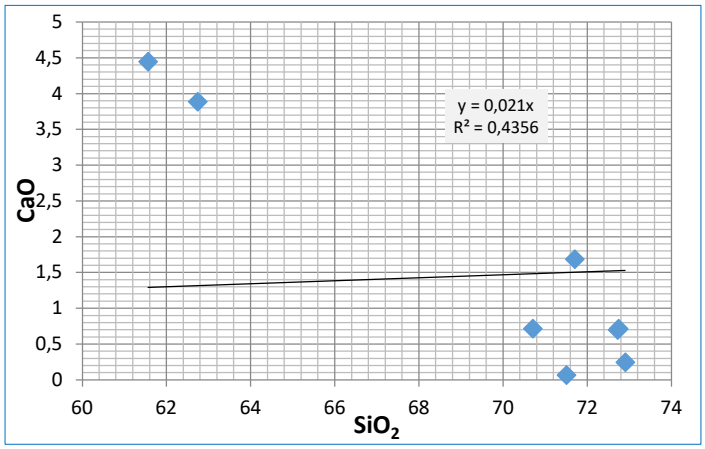

Fig. 33. SiO_2 against CaO

Fig. 38. shows the scattered diagram showing the concentration pattern of the Major Oxides. The major oxides of the Mar.NP 9 and Mar.OP 10 samples, expressed in weight percent (wt.%), are presented in Table 8. The results show significant variation in oxide concentrations, reflecting differences in mineralogical composition and potential

suitability for industrial applications. Silica (SiO_2): Mar.NP 9 contains 0.71 wt.% while Mar.OP 10 contains 0.90 wt.%. These values are below the FMS (RMR & DC) 2011 standard of 5%, indicating relatively low quartz content.

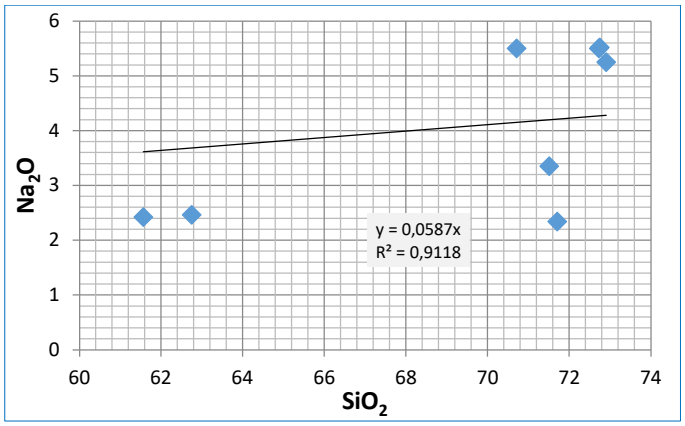

Fig. 34. SiO_2 against Na_2O

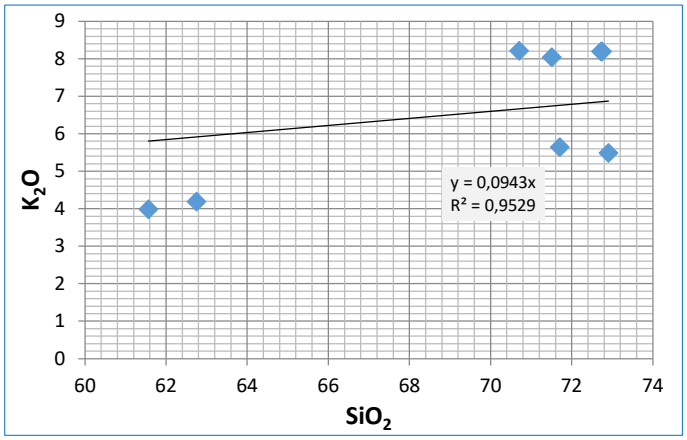

Fig. 35. SiO_2 against K_2O

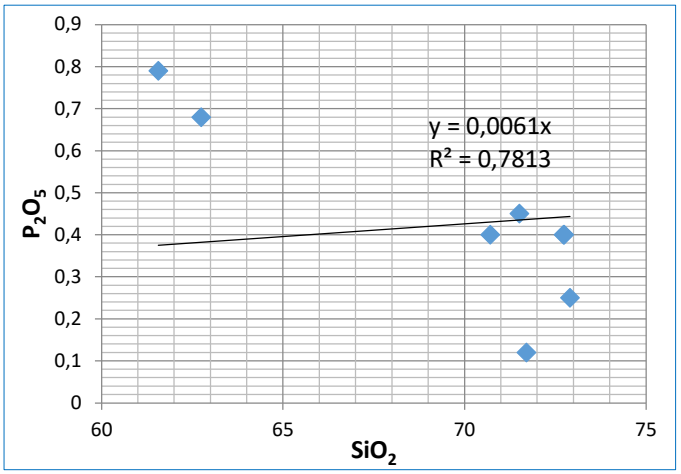

Fig. 36. SiO_2 against P_2O_5

Titanium dioxide (TiO_2): Both samples have very low concentrations (0.01–0.02 wt.%), which is negligible and does not impact their industrial use. Alumina (Al_2O_3): Concentrations are 0.52 wt.% in Mar.NP 9 and 0.07 wt.% in Mar.OP 10, slightly below the FMS standard of 1.25%. Iron oxide (Fe_2O_3): Values range from 0.18 to 0.34 wt.%, slightly below the standard (2%), suggesting minimal iron contamination.

Manganese oxide (MnO), Sodium oxide (Na_2O), and Potassium oxide (K_2O): All show trace amounts (<0.1 wt.%), except K_2O in Mar.OP 10 (0.08 wt.%). These low values indicate the samples are largely free of alkali and transition metal oxides. Magnesia (MgO): Concentrations are 0.35–0.42 wt.%, slightly below the 6% standard, implying low magnesium content. Calcium oxide (CaO): The dominant oxide in both samples, 54.75 wt.% in Mar.NP 9 and 54.01 wt.% in Mar.OP 10, consistent with high-calcium materials such as limestone. Both are within the standard (54.28 wt.%).

Table 7. Comparison of oxides (Wt%) in sample 8, with that of Okpella (Omoruyi et al., 2022)

No	Major Elements %	Pgm 8	Pgm C	Pgm D
1	SiO_2	72.72	70.58	69.38
2	TiO_2	0.02	0.042	0.802
3	Al_2O_3	15.17	16.98	16.05
4	Fe_2O_3	0.48	0.74	4.59
5	MnO	0.02	0.032	0.08
6	MgO	0.08	0.108	0.44
7	CaO	0.70	0.898	0.72
8	Na_2O	5.50	4.334	1.78
9	K_2O	8.20	6.672	1.41
10	P_2O_5	0.40	0.019	1.54
11	LOI	0.20		

Phosphorus pentoxide (P_2O_5): Trace amounts (0.01–0.02 wt.%) suggest minimal phosphate content, below the 1% standard. Loss on ignition (LOI): High values of 42.01 wt.% (Mar.NP 9) and 43.72 wt.% (Mar.OP 10) indicate significant volatile content, including structural water and carbonates as shown in Table 8 and Fig. 38. The samples are calcium-rich and low in silica, alumina, and other trace oxides, indicating they are predominantly carbonate in nature.

High LOI values reflect substantial volatile loss upon heating, typical of limestone or dolomitic materials. The minor concentrations of TiO_2, Fe_2O_3, and alkalis suggest minimal contamination by silicate or mafic minerals. Overall, both samples meet FMS standards for calcium content, making them suitable for cement or lime production, but the low silica content limits applications requiring siliceous material as shown plate 10 and 11.

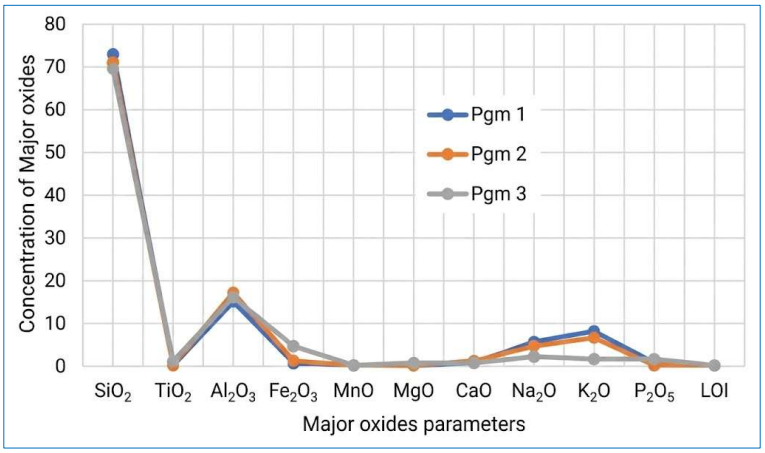

Fig. 37. Scatter diagram showing the concentration pattern of the major oxides of pegmatite

Table 8. Comparison of oxides (Wt%) in sample 9 and 10, with that of Obhu Hill Marble Deposit, Okpella (Sanni et al., 2018)

No	Major Elements, Wt. %	Mar.NP 9	Mar. OP 10	E	F	FMS (RMR &DC) Standard 2011(%)
1	SiO_2	0.71	0.90	8.54	7.43	5
2	TiO_2	0.01	0.02	0.01	0.01	-
3	Al_2O_3	0.52	0.07	3.11	3.46	1.25
4	Fe_2O_3	0.34	0.18	1.85	2.51	2
5	MnO	0.01	0.01	0.01	0.01	-
6	MgO	0.35	0.42	5.24	6.11	6
7	CaO	54.75	54.01	71.63	76.53	54.28
8	Na_2O	0.01	0.02	0.01	0.01	-
9	K_2O	0.01	0.08	2.75	1.22	-
10	P_2O_5	0.01	0.02	0.71	0.74	1
11	LOI	42.01	43.72			

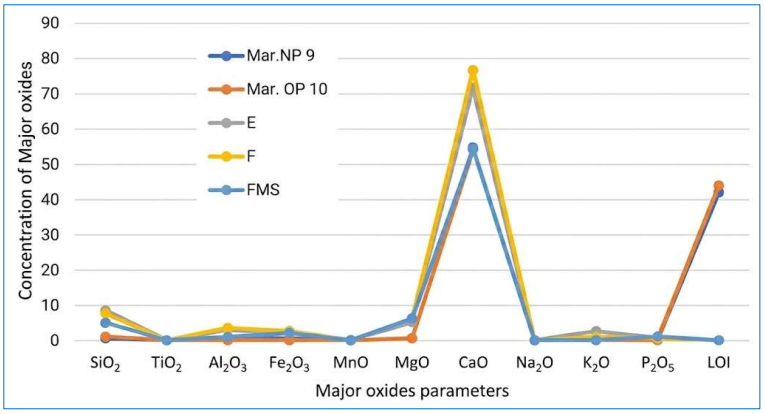

Fig. 38. Scatter diagram showing the concentration pattern of the major oxides of marbles

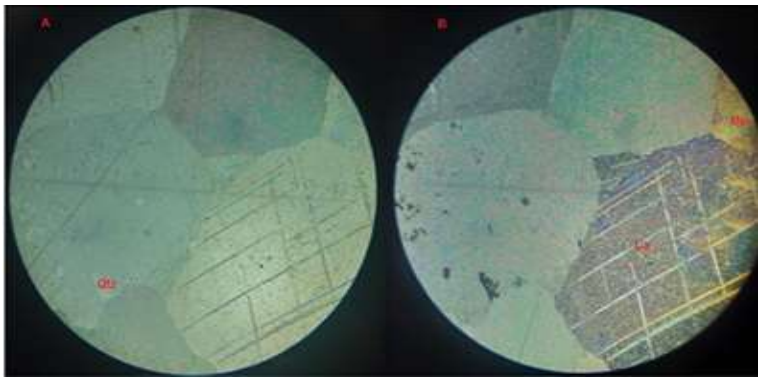

Fig. 39. Photomicrograph of Sample 9, Marble (a) under PPL and (b) under XPL x40; op-opaque, Qzt-Quartz, Mc-Microline, Ca-Calcite

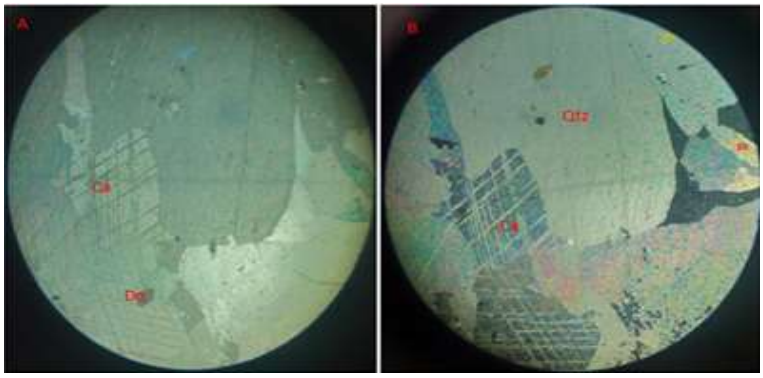

Fig. 40. Photomicrograph of Sample 10, Marble (a) under PPL and (b) under XPL x40; op-opaque, Qzt-Quartz, Mc-Microline, Ca-Calcite, Do-Dolomite

5.9. Petrography

Petrographic examination shows that quartz and feldspars (microcline) dominate the granites and pegmatites, with biotite, hornblende, and muscovite as accessory minerals. Charnockites contain quartz, feldspar, biotite, and orthopyroxene (hypersthene), indicating high-temperature formation. Pegmatites exhibit coarse-grained quartz, microcline, mica, and garnet. Marbles consist predominantly of calcites with minor silicate impurities.

6. Discussion

6.1. Petrogenesis and Tectonic Setting

Geochemical discrimination diagrams (TAS, K_2O–SiO_2, A/CNK–A/NK) classify the granitoids as high-K calc-alkaline to shoshonitic, peraluminous rocks emplaced within a passive continental margin setting. The peraluminous nature suggests derivation from partial melting of metasedimentary crustal sources during Pan-African tectonism (White and Chappell, 1977; Frost et al., 2001).

6.2. Economic Implications

The high CaO content of the marbles supports their suitability for cement and lime production. The granites and charnockites, characterized by high silica and feldspar content, are suitable for construction materials, ceramics, and glass industries. Pegmatites may host economically valuable minerals such as feldspar, mica, and gemstones.

7. Conclusions

The Basement Complex rocks around Afokpella are products of Pan-African magmatic and metamorphic processes, involving crustal melting and tectonic reworking. These rocks are predominantly silica- and calcium-rich, with a high proportion of feldspar. Integrated geochemical, petrographic, and statistical analyses reveal that the granitoids are felsic, ranging from peraluminous to weakly peralkaline, emplaced within a passive margin tectonic setting, while the marbles correspond to recrystallized carbonate sediments originally deposited in shallow marine environments. Correlation and statistical analyses suggest that the major oxides share common sources, with minor lithological heterogeneity across the study area. Petrographic and geochemical data further indicate the presence of felsic S-type granites, charnockites, and marbles, characteristic of a Pan-African Basement Complex rock. These rocks demonstrate considerable industrial potential, suitable for applications in glass, ceramics, and cement production, while their geochemical signatures provide insights into provenance and tectonic evolution. Based on these findings, it is recommended that government-led programs be implemented, including the establishment of processing plants, to enhance the economic and financial well-being of communities residing in and around the study area.

References

Ogunyele, A., Adegbuyi, O., Odindu, M., Erinfolami, T., 2017. Geochemical characteristics and petrogenesis of basement rocks in Idoani area, southwestern Nigeria. Journal of African Earth Sciences 129, 400-415. https://doi.org/10.14419/ijag.v5i2.8377.

Ajibade, A.C., Wright, J.B., 1989. The Togo–Benin–Nigeria shield: Evidence of crustal aggregation in the Pan-African belt. Tectonophysics 165 (1–4), 125-137.

Cox, K.G., Bell, J.D., Pankhurst, R.J., 1979. The interpretation of Igneous rocks. George Allen and Unwin. P. 2.

Dada, S.S., 2006. Petrology and geochemistry of the Nigerian Basement Complex: Implications for Pan-African tectonics. Journal of African Earth Sciences 44 (1), 123-136.

Dyar, M.D., Gunter, M.E., 2008. Optical mineralogy and the characterization of silicate and ferromagnesian minerals. Journal of Petrological Microscopy 17 (2), 33-47.

Frost, B.R., Frost, C.D., Czamanske, G.K., 2001. Geochemical and petrological constraints on granite genesis in Pan-African terranes. Lithos 56 (1-2), 121-145.

Joplin, G.A., 1968. The Shoshonite Association: A Review. Journal of the Geological Society of Australia 15 (2), 275-294.

London, D., Kontak, D.J., 2012. Granitic pegmatites: Scientific wonders and economic bonanzas. Elements 8 (4), 257-261.

McNamee, M.S., Gunter, M.E., 2014. Mineral identification in thin section: Optical properties and petrographic techniques. Mineralogical Society Publications 88, 57-75.

Ogunyele, A.C, Obaje, S.O, Akingboye, A.S, Adeola, A.O, Olufunmilayo, A.T., 2020. Petrography and geochemistry of Neoproterozoic charnockite–granite association and Metasedimentary rocks around Okpella, southwestern Nigeria.

Okeke, P.0., Akinnagbe, L., Anike, L,O., 1988. Major and Minor Element Evaluation of the Igarra Granite. Journal of Mining and Geology 24 (1), 101-106.

Omang, J., 2019. Geochemistry of feldspar and quartz-rich rocks for industrial applications. Industrial Minerals Research Journal 14 (3), 45-59.

Omoruyi1, D.I., Ilevbare, M., Ehinlaiye, A.O., Akujieze, C.N., 2022. Geochemical Discriminant for Provenance Characterization of Some Clay Deposits in Edo State, Nigeria.

International Journal of Earth Sciences Knowledge and Applications 4 (3), 407-418.

Peccerillo, A., Taylor, S.R., 1976. Geochemistry of Eocene Calc-Alkaline Volcanic Rocks from the Kastamonu Area, Northern Turkey. Contributions to Mineralogy and Petrology 58, 63-81.

Rahaman, M.A., 1988. Recent Advances in the Study of the Basement Complex of Nigeria. In Precambrian Geology of Nigeria. Geological Survey of Nigeria, Kaduna South, Pp. 11-43.

Roser, B.P., Korsch, R.J., 1986. Determination of tectonic setting of sandstone–mudstone suites using SiO_2 content and K_2O/Na_2O ratio. Journal of Geology 94, 635-650.

Sanni, E.B., Yusuf, I., Umoru, A., Osaghae, S.O., Sule, T.U.N., Yemi, O., 2018. Geochemical investigations of a Portion of Obhu Hill Marble Deposit Okpella, Edo-State, Nigeria 3 (2), 1-5.

Shand, S.J., 1943. Eruptive Rocks. Their genesis, composition, classification and their relation to ndore-deposit with a chapter on meteorite. 2 (Eds). John Wiley and Sons, New York, 1- 44.

Taylor, S.R., McLennan, S.M., 1981. The geochemical evolution of the continental crust. Reviews of Geophysics 19 (2), 103-136.

White, A.J.R., Chappell, B.W., 1977. Ultrahigh temperature metamorphism and granite formation in the Australian continent. Contributions to Mineralogy and Petrology 62, 301-312.

Winter, J.D., 2014. Principles of Igneous and Metamorphic Petrology: Pearson New International Edition. Pearson Education Limited, Harlow, UK.